Catalysis Letters
https://doi.org/10.1007/s10562-018-2647-2

Synthesis of Fe–Co–Ce/Zeolite A-3 Catalysts and their Selectivity to Light Olefins for Fischer–Tropsch Synthesis in Fixed-Bed Reactor

Reza Nohtani[1] · Ali Akbar Mirzaei[1] · Amir Eshraghi[1]

Received: 11 November 2018 / Accepted: 13 December 2018

Abstract

In the present work, Fe–Co–Ce/Zeolite A-3 catalysts were prepared, using the impregnation method and applied in Fischer–Tropsch Synthesis (FTS). The catalyst's performance was investigated by changing the catalyst's composition and process conditions. Increased pressure from 2 to 10 and H_2/CO ratio from 1 to 4 were accompanied by decreased olefin to paraffin proportion and increased C_4^+ production. Decline in the GHSV led to decrease in methane and light olefin generation, and a significant increase in the number of carbon in the products. The catalysts were characterized by SEM, BET, STA and XRD. Catalyst composition was changed with different loading of support (Zeolite A-3) and metals (Fe, Co, Ce). Finally, 45%Fe–45%Co–10%Ce/60%Zeolite A-3 catalyst was judged to be the best composition to obtain the optimal operation conditions (high selectivity towards light olefins and low selectivity towards methane, simultaneously).

Graphical Abstract

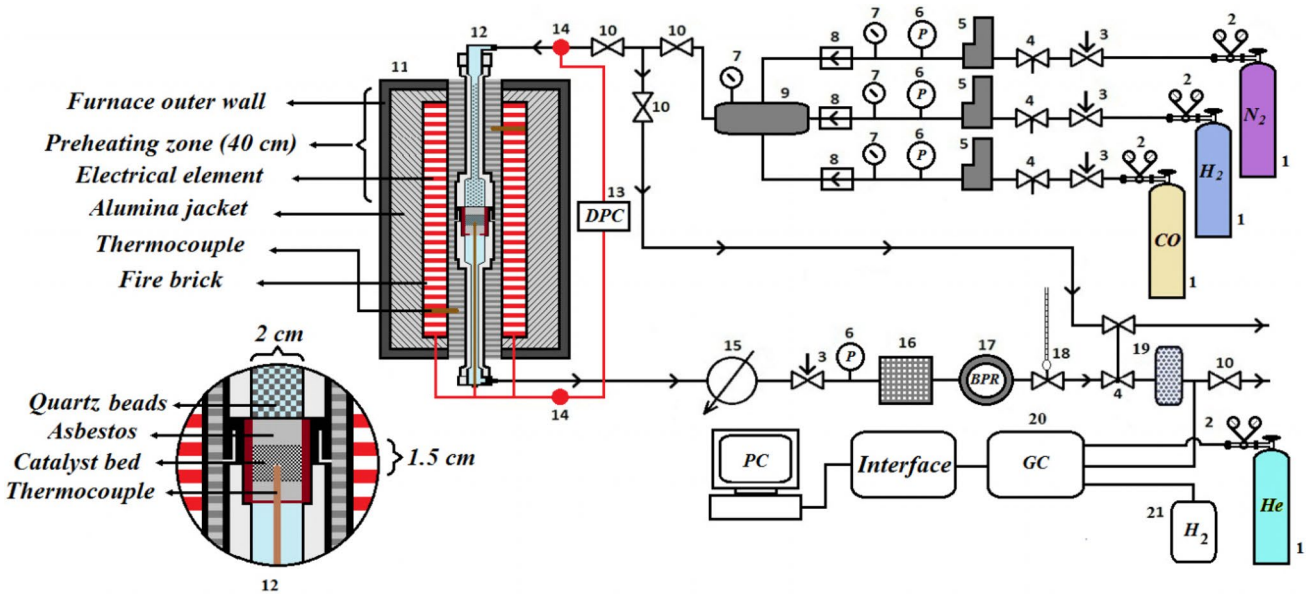

Keywords Catalyst composition · Reaction conditions · FT reaction · Light olefins selectivity

1 Introduction

The abundant human use of non-renewable energy sources such as coal, petroleum and natural gas has led to concerns about environmental change, global warming and

✉ Ali Akbar Mirzaei
mirzaei@hamoon.usb.ac.ir

[1] Department of Chemistry, Faculty of Sciences, University of Sistan and Baluchestan, 98135-674 Zahedan, Iran

Published online: 07 January 2019

living organisms. The problem has made renewable energy an attractive topic and better supported by governments. On the other hand, these non-renewable resources will be exhausted in the near future. So, it is necessary to use renewable sources and green fuels [1]. Synthesis gas produced by biomass gasification is used as feed in FT reaction and for producing a variety of fuels and valuable chemicals. FT fuel is environmentally friendlier than fuel obtained from crude oil [1–4]. In FTS, syngas (mixture of $H_2 + CO$) is converted to a wide range of products such as alkanes, alkenes, alcohols, aldehydes and ketones [1, 5, 6]. Since this is a catalytic process, for optimization, the properties of the catalysts such as physio-chemical and mechanical, as well as particle size and shape must be taken into consideration [7]. In order to control FTS towards desired products, many studies have been carried out. This action can be performed by choosing proper reactor, catalyst composition and operating conditions [8–11]. In general, FT commercial reactors can be divided into three basic classes: FT slurry reactor, fluid bed and fixed bed [12]. The most common catalysts are used for the FTS of group 8 metals such as iron, cobalt, ruthenium and nickel [11, 13, 14]. Among the catalysts for commercial applications, are those based on iron and cobalt [9, 15, 16]. The effects of Ce as promoter over Co and Fe-based catalysts on activity and selectivity were studied [17–22]. Fatima Pardo-Tarifa et al. [21] reported that the presence of Ce causes decrease in Co-based catalyst, reduction in temperature and improvement of the catalyst activity. Wen-Ping Ma et al. [19] also reported that Ce promoter improved the Co-based catalyst activity with high methane selectivity. In the study of Sun et al. [22], it was reported that addition of Ce to Fe-based catalyst resulted in improved activity and selectivity to C_5^+ hydrocarbons. Sergio-Rojas et al. [17] in their studies on Fe-based catalysts, it was shown that Fe catalyst modified with Ce as a promoter activated under CO continuous flow, subsequently, sped up the stabilization active intermediate of carbon compounds. Generally, to achieve the thermal and mechanical stability, high surface area, suitable dispersion of metals, etc. the presence of support is necessary [23, 24]. Traditional porous supports are Al_2O_3, SiO_2 or TiO_2 [25, 26]. Although zeolite has been used as a support in FT catalysts for fabrication of long chain liquid fuels [27, 28], it seems reasonable that by controlling the operation condition (for example low pressure), the selectivity of light olefins is considered as a goal. The aim of this study was to investigate catalyst composition (metals and support loading) and process conditions effect on the catalyst activity. The structural investigation was done by applying Simultaneous Thermal Analysis (STA), Brunauer–Emmett–Teller (BET) surface area measurements, X-ray diffraction (XRD) and scanning electron microscopy (SEM).

2 Methods and Materials

2.1 Catalyst Synthesis

In this work, an impregnation method was used for supported Fe–Co–Ce/Zeolite A-3 catalyst synthesis. To obtain the desired catalyst composition, the required values of Cobalt (II) nitrate hexahydrate (purity of 97% Merck), Iron (III) nitrate nonahydrate (purity of 98% Merck) and Cerium (III) nitrate hexahydrate (purity of 98.5% Merck) were mixed in minimum amount of distilled water. The meshed (No. 150) Zeolite A-3 support was calcined for 6 h at 600 °C in air before impregnation. The solution was prepared from the metals that were directly impregnated onto calcined Zeolite A-3 and it was dried for 6 h in an oven at 120 °C. Finally, in order to perform the calcination, the dried catalyst was placed in the furnace at 600 °C for 6 h.

2.2 Characterization of Catalysts

2.2.1 X-ray Diffraction (XRD)

X-ray diffraction (XRD) technique was used to identify the catalyst phases. In order to perform this analysis, an ADVANCE D8 device (made in Germany) and Cu–Ka radiation were used. Catalyst phases were identified by matching the experimental patterns with standard samples diffraction patterns.

2.2.2 BET Measurements

The BET method was used to specify the surface area of the catalyst samples. BET measurements were taken by using Quantachrome Nova 2000 (made in USA). Prior to the analysis of BET, all the catalyst samples (precursor, calcined before and after the reaction) were placed under nitrogen atmosphere for 4 h at a temperature of 300 °C.

2.2.3 Simultaneous Thermal Analysis (STA)

To determine catalyst precursor mass changes caused by temperature changes, STA technique was used. This technique includes two simultaneous tests: Thermal Gravimetric Analysis (TGA) and Differential Scanning Calorimetry (DSC) tests. The TGA was used to indicate sample weight variations and DSC for specify endothermic or exothermic change in sample's mass. In this work, Rheometric Scientific STA 1500+ was used for simultaneous TGA and DSC.

2.2.4 Scanning Electron Microscopy (SEM)

The morphology of catalyst was observed using A Cambridge S-360 scanning electron microscope device.

2.3 Catalytic Tests

A fixed bed reactor was used to perform catalytic tests. Details and setup of the reactor system are provided in previous work [29]. Briefly, in each experiment, one gram of calcined catalyst was put into the reactor. Prior to the start of reaction, the fresh catalyst was reduced in pure hydrogen (H_2) stream for 14 h (T = 400 °C, P = 2 bar, flow rate = 37.5 ml/min). These reduced conditions were used for all samples in the next sections. The FT catalytic tests were carried out under the following operating conditions: T = 300–360 °C, P = 2–10 bar, gas hourly space velocity (GHSV) = 1800–4200 h^{-1} and molar ratio of H_2/CO = 1/1–4/1. To calculate CO conversion and selectivity, Eqs. 1 and 2 were used, respectively.

$$\text{CO Conversion } (\%) = \frac{\text{Mol of CO}_{in} - \text{Mol of CO}_{out}}{\text{Mol of CO}_{in}} \times 100 \quad (1)$$

$$\text{Selectivity } (\%) = \frac{n_i C_i}{\sum n_i C_i} \times 100 \quad (2)$$

n_i is carbon number of hydrocarbon i.

3 Results and Discussion

At the beginning of the reaction, all the catalyst's active sites were available, so, the catalyst had its highest activity. In this state, the catalyst's behavior was not stable and shifted to a near constant conversion [30–39]. Therefore, the data could not be provided. To find the best time to record data after the beginning of the reaction, CO convertion was calculated at different times. As shown in Fig. 1, after 10 h, the catalyst reached a steady state and the CO conversion was almost constant. 10 h was considered as the optimum time and all the data in this work were recorded 10 h after the beginning of the reaction.

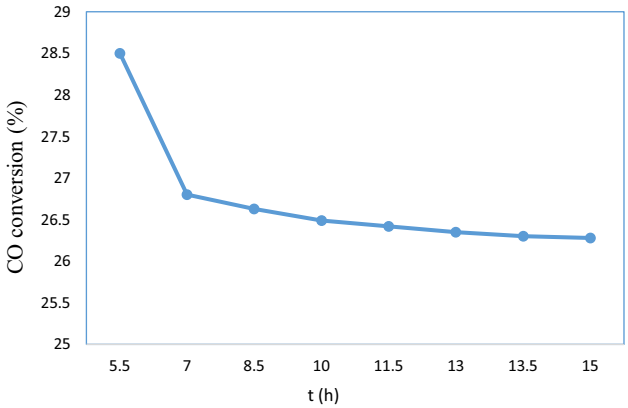

Fig. 1 Effects of contact time on CO conversion by Fe–Co–Ce/Zeolite A-3 catalyst (catalyst 45%Fe–45%Co–10%Ce/70%Zeolite A-3, P = 2 bar, T = 320 °C, molar ratio of H_2/CO = 2/1,GHSV = 3600 h^{-1})

3.1 Catalyst Composition Impact on the Light Olefins Selectivity

3.1.1 Effect of Ce Content

In this step, Ce ratio in catalysts preparation was changed. The selectivity plot of catalysts with different amounts of cerium is presented in Fig. 2. First, the catalyst 47.5%Fe–47.5%Co–5%Ce/70%Zeolite A-3 (No. 1), Catalyst 45%Fe–45%Co–10%Ce/70%Zeolite A-3 (No. 2), catalyst 42.5%Fe–42.5%Co–15%Ce/70%Zeolite A-3 (No. 3) and catalyst 40%Fe–40%Co–20%Ce–70%Zeolite A-3 (No. 4) under the same reduction and operating conditions (P = 2 bar, T = 320 °C, molar ratio of H_2/CO = 2/1 and GHSV = 3600 h^{-1}) were exposed to FT reaction. The optimum amount of cerium was chosen taking into account, increased selectivity of light olefins or olefin to paraffin ratio and suppression of methane formation. The selectivity of catalysts (No. 1–No. 4) towards light olefins was 24.86, 29.93, 27.10, 24.98%, and methane was calculated as 47.11, 43.46, 51.08 and 49.48%, respectively. Catalyst number 2 had the highest selectivity for light olefins (29.93%) and the least selectivity was for methane (43.46%). Therefore, the molar ratio of 10% of cerium was selected as the optimal ratio. The findings of BET for all the calcined catalysts are represented in Table 1. As indicated in the table, the BET measurements' results such as pore volume and surface area for catalysts with various Ce loading were different. It is clear that these features are affected by increase in the Ce molar ratio. High activity of No. 2 catalyst can be explained by surface areas data. Between catalysts, No. 2 catalyst had more surface area; that was why 10% of cerium was chosen as an optimum molar ratio.

3.1.2 Effect of Fe/Co Molar Ratio on the Catalyst Performance

Like the previous step, Fe–Co ratio was changed in the optimal amount of cerium obtained in the previous section. Catalysts' performances are indicated in Fig. 3. In the previous section, optimum molar ratio of cerium (10%) was chosen. Now, the optimum amount of Fe–Co is sought. FT reaction was carried out under similar process conditions (P = 2 bar, T = 320 °C, molar ratio of H_2/CO = 2/1

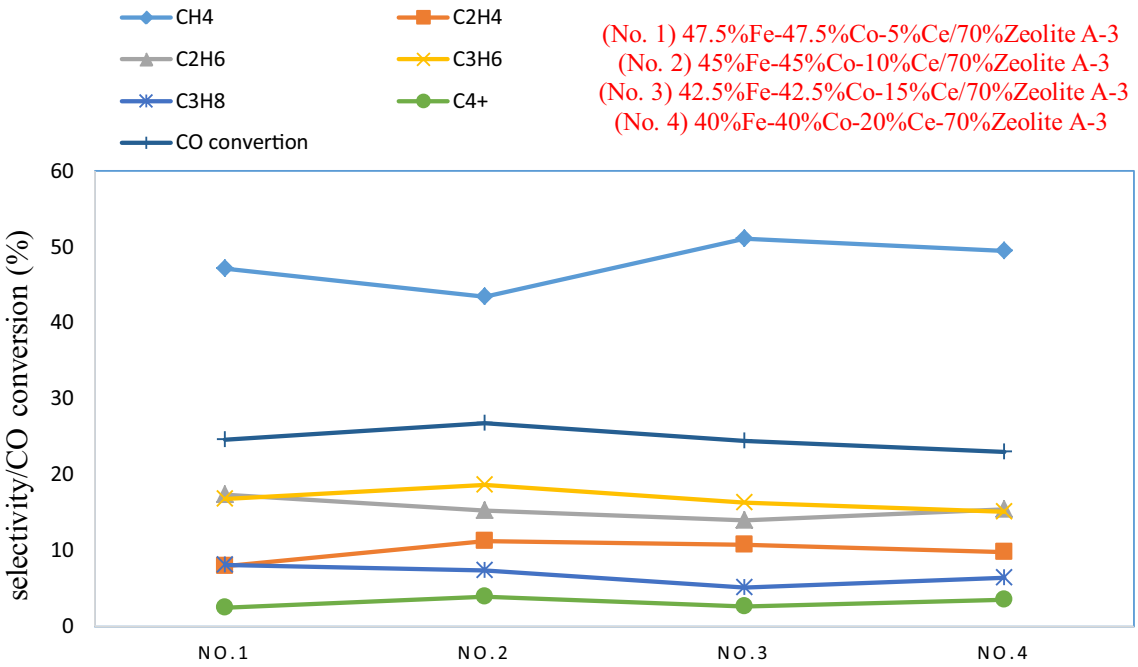

Fig. 2 Effects of Ce content on the catalytic performance (P = 2 bar, T = 320 °C, molar ratio of H_2/CO = 2/1, GHSV = 3600 h^{-1})

Table 1 BET surface area measurements for catalysts with different Ce contents

Calcined catalysts	Surface areas (m^2/g)	Pore volume (cm^3/g)
47.5%Fe–47.5%Co–5%Ce/70%Zeolite A-3		
No. 1	50.14	0.017
45%Fe–45%Co–10%Ce/70%Zeolite A-3		
No. 2	67.26	0.025
42.5%Fe–42.5%Co–15%Ce/70%Zeolite A-3		
No. 3	60.73	0.020
40%Fe–40%Co–20%Ce–70%Zeolite A-3		
No. 4	58.42	0.020

and GHSV = 3600 h^{-1}) on the catalysts with different Fe/Co ratios. Catalysts: 15%Fe–75%Co–10%Ce/70%Zeolite A-3 (No. 5), 30%Fe–60%Co–10%Ce/70%Zeolite A-3 (No. 6), 45%Fe–45%Co–10%Ce/70%Zeolite A-3 (No. 7), 60%Fe–30%Co–10%Ce/70%Zeolite A-3 (No. 8) and 75%Fe–15%Co–10%Ce/70% Zeolite A-3 (No. 9) were shown to have different behaviors. The results are shown in Fig. 3 increase in molar ratio of iron from 15 to 75% increased methane production from 37.78 to 46.43% and C_4^+ production decreased from 13.88 to 2%. Finally, the ratio of 45%Fe–45%Co was selected as Fe–Co optimum ratio. This selection is due to the maximum selectivity of light olefins and minimum of C_4^+ production. Figure 4 shows XRD patterns for calcined catalysts, including different Fe–Co loading. The actual detected phases for them were Fe_3O_4 (cubic-orthorhombic), Ce_2O_3 (hexagonal), Fe_2O_3 (rhombohedral), Co_3O_4 (cubic) and Ce_3O_4 (hexagonal). Although, the phases observed were similar, the relative intensity of the peaks was different.

3.1.3 Effect of Support Loading

In addition to metals, support properties such as surface area and distribution, volume and diameter of pores can influence the catalyst activity and selectivity [40, 41]. In this work, Zeolite A-3 was used as catalyst support. After optimizing the molar ratio of metals, the support loading impact on the performance of 45%Fe–45%Co–10%Ce/xZeolite A-3 catalyst in the synthesis of FT for the production of light olefin was investigated. Different amounts of Zeolite A-3 (50 [No. 10], 60 [No. 11], 70 [No. 12], 80 [No. 13] and 90% [No. 14]) were loaded in catalyst preparation. All catalysts were reduced and FT reaction was started under the following conditions (P = 2 bar, T = 320 °C, molar ratio of H_2/CO = 2/1 and GHSV = 3600 h^{-1}). The results are displayed in Fig. 5. The obtained results show that decrease in the amount of support from 90 to 50% did not significantly change CO conversion (about 25.2–27.3%), while selectivity for light olefins increased from 9.82 to 28.95%. Among the amounts of support loading, 60% support had maximum selectivity to light olefins. Finally, catalyst with optimum amounts of metals and support were determined. The 45%Fe–45%Co–10%Ce/60%Zeolite A-3 catalyst

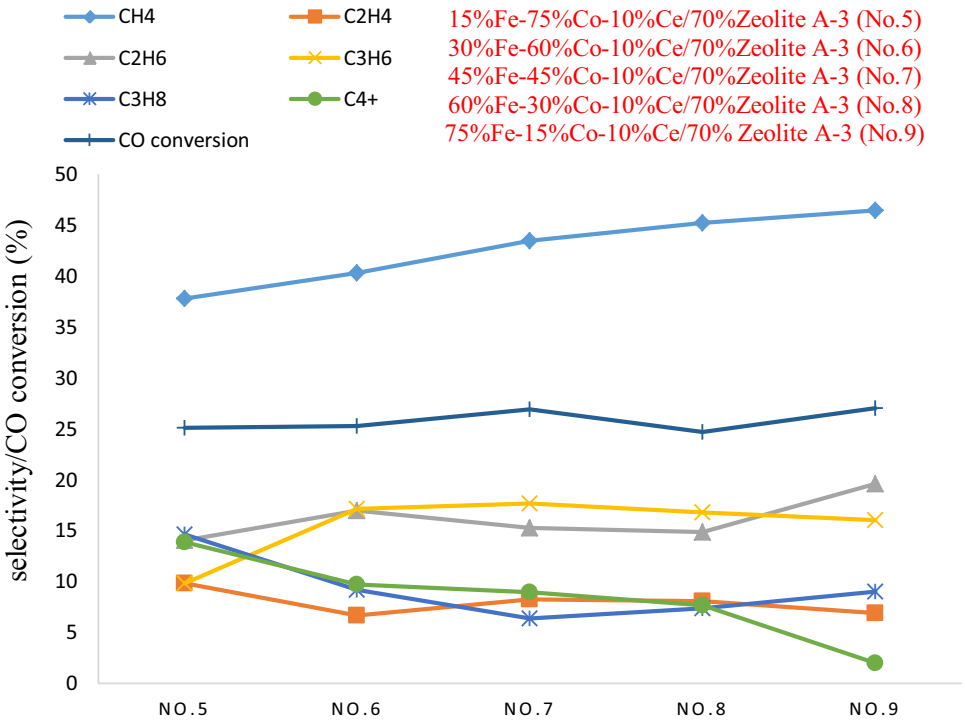

Fig. 3 Effect of Fe/Co molar ratio on the catalytic performance (P = 2 bar, T = 320 °C, molar ratio of H_2/CO = 2/1 and GHSV = 3600 h^{-1})

was considered as the optimum catalyst for the following sections.

3.2 Impact of Operational Conditions

In addition to catalyst composition, reaction conditions play an important role on activity and performance of catalyst in FT reaction. In order to find the optimum operating condition, reaction conditions such as T, P, GHSV and feed ratio were varied in FT reaction on the optimum catalyst.

3.2.1 The Temperature Impact

Generally, increase in temperature enhances the catalyst performance but too high or low temperatures are not appropriate for the reaction [42]. To study the effects of reaction temperature, the optimum catalyst was investigated at 300–360 °C under same situations (P = 2 bar, molar ratio of H_2/CO = 2/1 and GHSV = 3600 h^{-1}). The results in Table 2 show that, by increasing the temperature from 300 to 360 °C, CO conversion significantly increased from 24.57 to 38.34%. This result is in agreement with [43–45]. At T = 300 °C, methane formation (35.77%) was low and both CO conversion (24.57%) and light olefins production (17.3%) were low. This can be because of absence of adequate energy at low temperatures to activate the reactant on the catalyst [29]. In other words, it can be said that a significant amount of the reactants did not react with each other. At temperatures 340 and 350 °C, CO conversion and methane formation as the undesired product are high, and also, olefins production is low. In addition to this, at high temperature, the catalyst can be deactivated by sintering, coke formation and carbon deposition [46, 47]. T = 340 °C was chosen as optimum temperature because of high selectivity to light olefins. The catalysts were characterized after reaction by SEM. SEM images of used catalysts at T = 340, 350, 360 °C are presented in Fig. 6. The images show that the catalyst at T = 340 °C (Fig. 6a), T = 350 °C (Fig. 6b) and T = 360 °C (Fig. 6c) have different morphologies. These images result show that at T = 350 and 360 °C, there are some agglomerations in used catalysts which may be due to sintering during the FT reaction, and coke formation.

3.2.2 Effect of Gas Hourly Space Velocity (GHSV)

The residence time has an inverse relationship with GHSV, as the residence time decreases with increase in GHSV. The GHSV impact on the efficacy of optimum catalyst was assessed under the same conditions (P = 2 bar, T = 340 °C, molar ratio of H_2/CO = 2/1) and variable GHSV = 1800, 2400, 3000, 3600 and 4200 h^{-1}. According to the data presented in Table 3, with a GHSV increase of 1800 to 4200 h^{-1}, production of heavy products decreased, due to reduction of the residence time. This result is in agreement with that of [48, 49]. In other words, decrease in GHSV causes a significant increase in the number of carbon in the products. On the other hand, light olefins production increased from 26.56 to 32.91%. It also increased methane

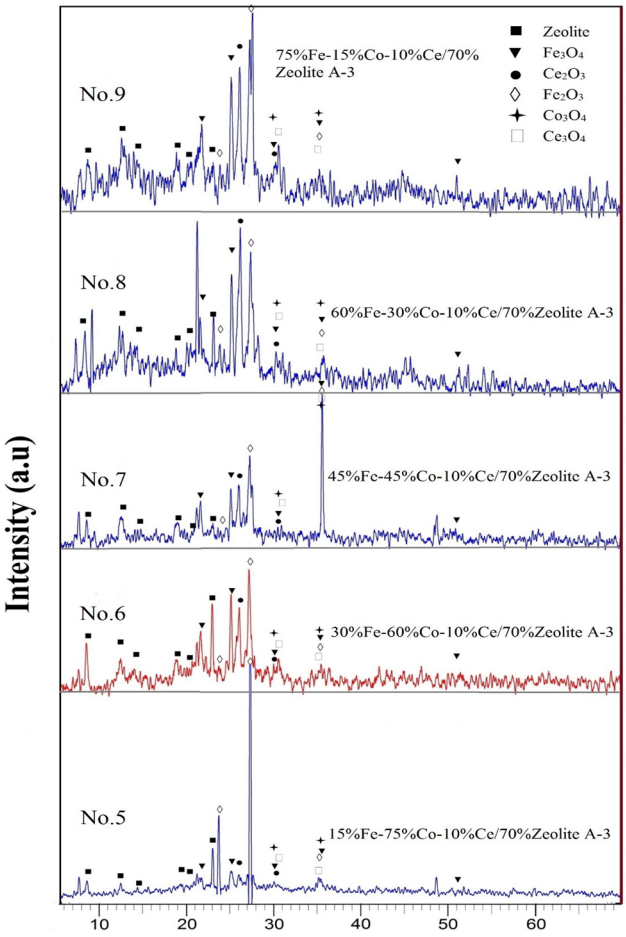

Fig. 4 XRD patterns of calcined catalysts No. 5, No. 6, No. 7, No. 8, No. 9

production from 39.19 to 54.69%. This behavior is expected due to less residence time for the feed and products over the catalyst. At low GHSV, feed (H_2+CO) had enough time for adsorption and reaction on the catalyst. Very low GHSV is not suitable because of the presence of external mass transfer limitation [50]. GHSV = 3600 h^{-1} was chosen as the optimum GHSV due to high production of light olefins (32.17%).

3.2.3 Effect of H_2/CO Molar Ratio

To evaluate H_2/CO molar ratio impact on the optimum catalyst selectivity and CO conversion, FT reaction was performed at T = 340 °C, P = 2 bar, GHSV = 3600 h^{-1} and the variable H_2/CO molar ratio from 1 to 4. Table 4 shows the effect of change in H_2/CO molar ratio on optimum catalyst selectivity and CO conversion. These results demonstrated that by changing H_2/CO molar proportion of 1–4, different selectivity towards any products and CO conversion were obtained. Table 4 shows that increase in the ratio of H_2/CO increased CO conversion, while selectivity for light olefins decreased. This behavior is in agreement with [51–53]. However, H_2/CO = 1 was considered as optimum molar ratio because of maximum selectivity to light olefin and minimum selectivity to CH_4.

3.2.4 Impact of Reaction Pressure on the Olefin to Paraffin Ratio

It is well known that total pressure plays pivotal role in FT reactions, and affects the catalyst performance directly. Increment in pressure has a positive impact on the catalyst selectivity [49]. In the current study, in order to investigate

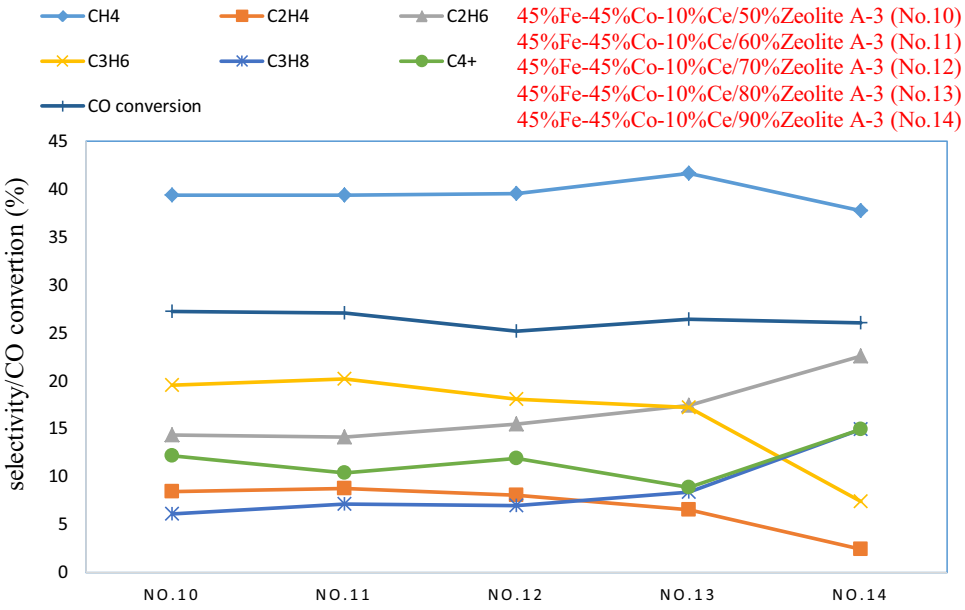

Fig. 5 Product selectivity and CO conversion of 45%Fe–45%Co–10%Ce catalyst with different support loadings (P = 2 bar, T = 320 °C, molar ratio of H_2/CO = 2/1 and GHSV = 3600 h^{-1})

Table 2 Temperature Effect on the selectivity of 45%Fe–45%Co–10%Ce/60%Zeolite A-3 catalyst (T = 300–360 °C, P = 2 bar, H_2/CO = 2/1 and GHSV = 3600 h^{-1})

T (°C)	Selectivity (%)						(%) CO conversion	Olefin/paraffin
	CH_4	C_2H_4	C_2H_6	C_3H_6	C_3H_8	C_4^+		
300	35.77	2.95	20.83	14.35	14.12	11.98	24.57	0.21
310	36.8	3.59	19.47	13.39	13.29	13.46	25.33	0.20
320	38.09	4.94	18.55	15.41	10.62	12.39	26.27	0.25
330	38.91	6.97	17.56	17.42	8.75	10.39	27.81	0.32
340	40.04	8.89	15.58	19.56	7.08	8.85	30.45	0.40
350	41.64	9.25	14.89	19.17	6.45	8.6	33.43	0.40
360	42.98	9.27	14.7	18.9	6.23	7.92	38.34	0.39

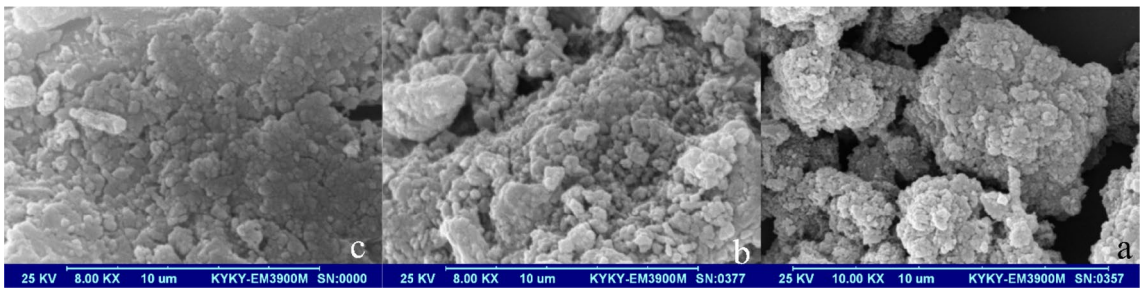

Fig. 6 SEM images of 45%Fe–45%Co–10%Ce/60%Zeolite A-3 catalyst at different temperatures **a** 340 °C, **b** 350 °C, and **c** 360 °C

Table 3 Effect of different GHSV on the 45%Fe–45%Co–10%Ce/60%Zeolite A-3 catalytic performance (T = 340 °C, P = 2 bar, H_2/CO = 2/1 and GHSV = 1800–4200 h^{-1})

GHSV (h^{-1})	Selectivity (%)						(%) CO conversion	Olefin/paraffin
	CH_4	C_2H_4	C_2H_6	C_3H_6	C_3H_8	C_4^+		
1800	39.19	7.52	15.07	19.04	6.84	12.34	32.3	0.36
2400	39.49	9.6	13.41	20.01	5.52	11.97	21.58	0.42
3000	40.23	10.72	12.56	20.21	4.77	11.51	16.64	0.45
3600	42.45	11.92	11.77	20.25	4.28	9.33	15.53	0.47
4200	54.69	13.05	9.59	19.86	2.51	0.3	13.64	0.49

Table 4 H_2/CO molar ratio effect of the 45%Fe–45%Co–10%Ce/60%Zeolite A-3 catalytic performance on distribution of products of FT reaction (T = 340 °C, P = 2 bar and GHSV = 3600 h^{-1})

H_2/CO ratio	Selectivity (%)						(%) CO conversion	Olefin/paraffin
	CH_4	C_2H_4	C_2H_6	C_3H_6	C_3H_8	C_4^+		
1	39.58	10.83	12.23	20.45	5.24	11.67	21.08	0.46
2	41.47	7.64	15.35	17.93	7.61	10	26.81	0.34
3	44.54	7.05	15.69	14.63	7.81	10.28	29.29	0.28
4	48.12	6.51	16.57	13.02	8.06	7.72	30.02	0.24

the effect of total reaction pressure on the catalytic activity and selectivity, FT reaction was carried out under similar conditions (molar ratio of H_2/CO = 1, GHSV = 3600 h^{-1} and T = 340 °C) and variable total pressure of reactants from 2 to 10 bar. The results are presented in Table 5. According to the results of Table 5, it is clear that with increase in the total pressure from 2 to 10 bar, significant increase in CO conversion (from 17.14 to 39.63) was observed and selectivity towards C_4^+ increased. Abbaslou et al. [54] explained that by increasing the pressure, the supercritical media indicates a liquid-like density that can increase the extraction from the catalyst pores. This phenomenon aids adsorption of carbon monoxide and hydrogen onto active sites, leading to increase in conversion. It is also evident that with increase in the total pressure in the range of 2–10 bar, the selectivity to light olefins decreased from 31.41 to 12.04%. P = 2 was selected as the optimum pressure because of highest selectivity to light olefins and olefin to paraffin ratio. XRD patterns of the catalyst samples (precursor, fresh calcined and used calcined) are displayed in Fig. 7. The actual phases that

Table 5 Effect of pressure on the 45%Fe–45%Co–10%Ce/60%Zeolite A-3 catalytic performance (T = 340 °C, $H_2/CO = 1/1$ and GHSV = 3600 h^{-1})

P (bar)	Selectivity (%)						(%) CO conversion	Olefin/paraffin
	CH_4	C_2H_4	C_2H_6	C_3H_6	C_3H_8	C_4^+		
2	38.92	11	12.78	20.41	5.42	11.47	17.14	0.46
3	39	8.15	14.98	19.52	7.21	11.14	18.78	0.38
4	38.83	6.28	15.95	17.98	8.75	12.21	19.92	0.32
5	38.6	4.79	16.73	16.43	10.23	13.22	23.11	0.27
6	39.18	3.71	17.79	14.71	11.65	12.96	25.72	0.23
7	39.09	3.06	17.97	13.6	12.29	13.99	28.3	0.20
8	38.76	2.31	18.09	11.91	13.51	15.42	31.99	0.17
9	38.62	2.04	18.41	11.14	13.78	16.01	34.91	0.15
10	39.06	1.74	18.85	10.3	14.74	15.31	39.63	0.14

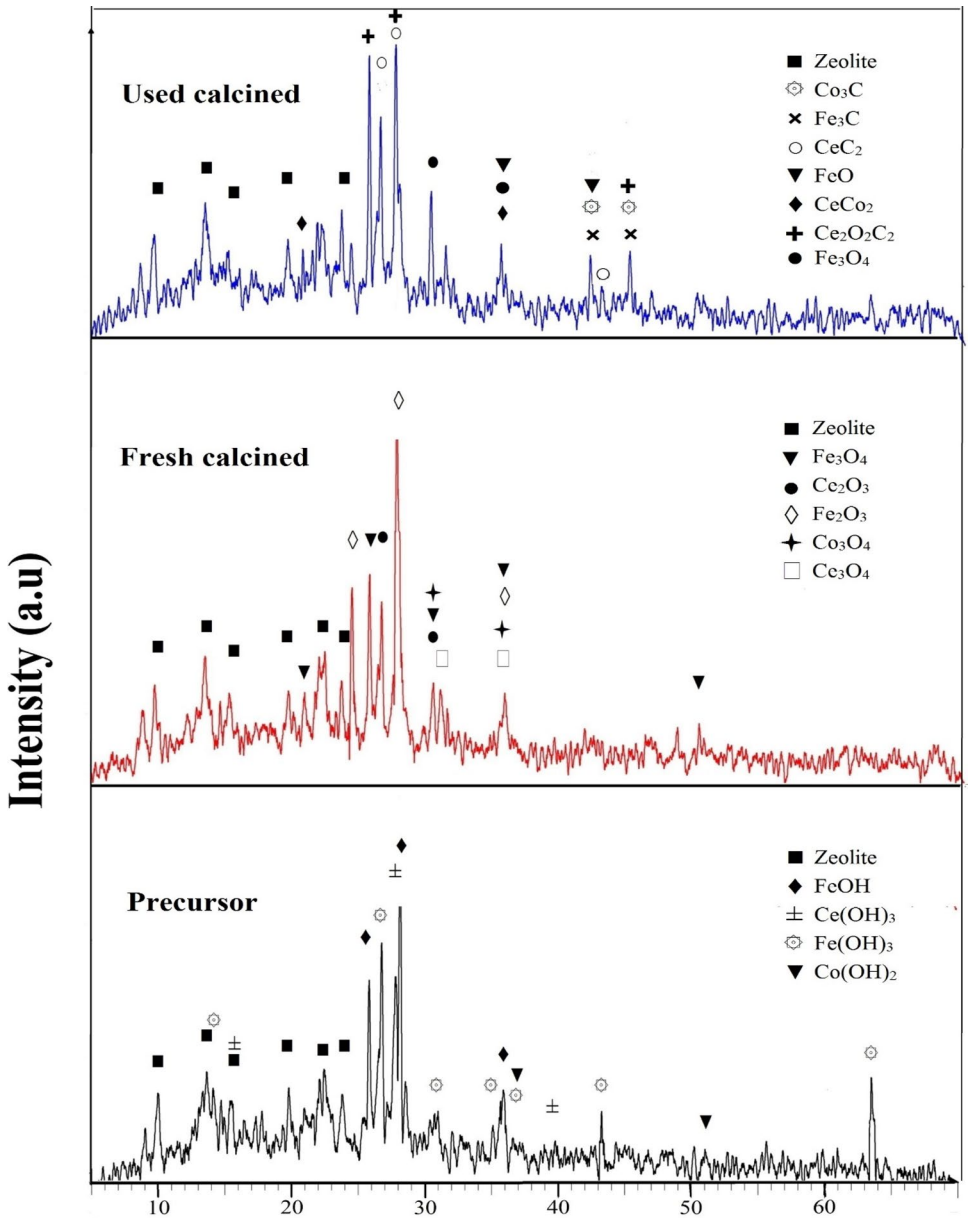

Fig. 7 XRD patterns of optimal catalyst (45%Fe–45%Co–10%Ce/60% Zeolite A-3) samples (precursor, fresh calcined and used calcined catalyst)

Table 6 BET measurements of optimum catalyst (45%Fe–45%Co–10%Ce/60%wt) samples (precursor, calcined and used calcined)

Precursor	Fresh calcined	Used calcined
Surface areas (m^2/g)		
63.45	68.15	34.06

were detected in the precursor were FeOH (orthorhombic), $Ce(OH)_3$ (hexagonal), $Fe(OH)_3$ (cubic) and $Co(OH)_2$ (hexagonal). The phases that were detected in the calcined catalyst before the reaction were Fe_3O_4 (cubic-orthorhombic), Ce_2O_3 (hexagonal), Fe_2O_3 (rhombohedral), Co_3O_4 (cubic) and Ce_3O_4 (hexagonal) which were different from the precursor. These results show that different phases detected in the precursor were transferred to oxidic phases. The calcined catalyst after the test had different phases [Co_3C (orthorhombic), Fe_3C (orthorhombic), CeC_2 (tetragonal), FeO (cubic), $CeCo_2$ (cubic), $Ce_2O_2C_2$ (hexagonal) and Fe_3O_4 (cubic)] compared to the calcined catalyst before the reaction. The calcined catalyst after the reaction had oxidic and carbidic phases, these are active phases for the FT reaction [55, 56]. BET measurements for both calcined catalyst (before and after reaction) and precursor are presented in Table 6. The data showed that the calcined catalyst before the start of the reaction had the greatest surface area. Used catalyst had lower surface area than calcined catalyst before the reaction, which might be due to sintering and coke formation. It is worth mentioning that one of the application of ZSM5 is in the Mobil/Badger process since 1980 [57]. One of the faced problems in this process is coking, and the different conditions required for regeneration. However, there are numerous studies that have illustrated a high resistance to coking of ZSM-5 [58–60]. Also, the results in this research demonstrated that under Fischer–Tropsch operating conditions (P = 2 bar, T = 320 °C, molar ratio of $H_2/CO = 2/1$ and GHSV = 3600 h^{-1}), the catalyst has a good stability. It is worth mentioning that there is a probability for coking at high temperatures (T = 360 °C, Sect. 3.2.1). Similar result was obtained for Co–Ce/zeolite in our previous study [61].

An optimal catalyst precursor was investigated by evaluating thermal behavior using TGA and DSC technique. TGA and DSC curves are presented in Fig. 8. As shown in TGA curve, a weight loss of 8 percentage was observed in the temperature from 80 until 360 °C. The initial weight loss happened at a temperature range of 80–180 °C, which can be attributed to the loss of physisorbed water and second mass loss in the temperatures 180–360 °C can be due to decomposition of the nitrate phase. The DSC spectrum of this sample also confirms the TGA result. As shown in Fig. 8, DSC spectra have two peaks. An endothermic peak appears at low temperatures, and is referred to as the loss of physisorbed water. Another endothermic peak appears at higher temperatures, which is related to decomposition of the nitrate phase.

4 Conclusion

The effect of operational conditions and catalyst composition on the selectivity over Fe–Co–Ce/Zeolite A-3 supported catalysts was studied. BET surface areas of catalysts showed that different amounts of cerium causes changes in surface areas of catalysts and catalyst with higher surface area has maximum olefin to paraffin ratio. Amounts of metals and support were variable finally, 45%Fe–45%Co–10Ce%/60%Zeolite A-3 catalyst was found to be the optimum catalyst because of its high selectivity towards light olefin and methane suppressed. Catalyst performance was also impacted by reaction condition such as pressure, temperature, GHSV and feed molar ratio. The SEM images showed that the catalysts were deactivated at a temperature higher than 340 °C by formation of coke and sintering, as well. The results of XRD showed that calcination caused the transformation of different phases of the hydroxide in the optimum precursor catalyst to oxidic phases. The TGA curve of optimum precursor catalyst showed two steps of mass loss at temperatures of 80–180 °C and 180–360 °C, corresponding to evaporation of physisorbed water, decomposition of the nitrate phase and stable oxide production, respectively. Optimal reaction conditions were found to be T = 340 °C, P = 2 bar, GHSV = 3600 h^{-1} and feed molar ratio = 1/1.

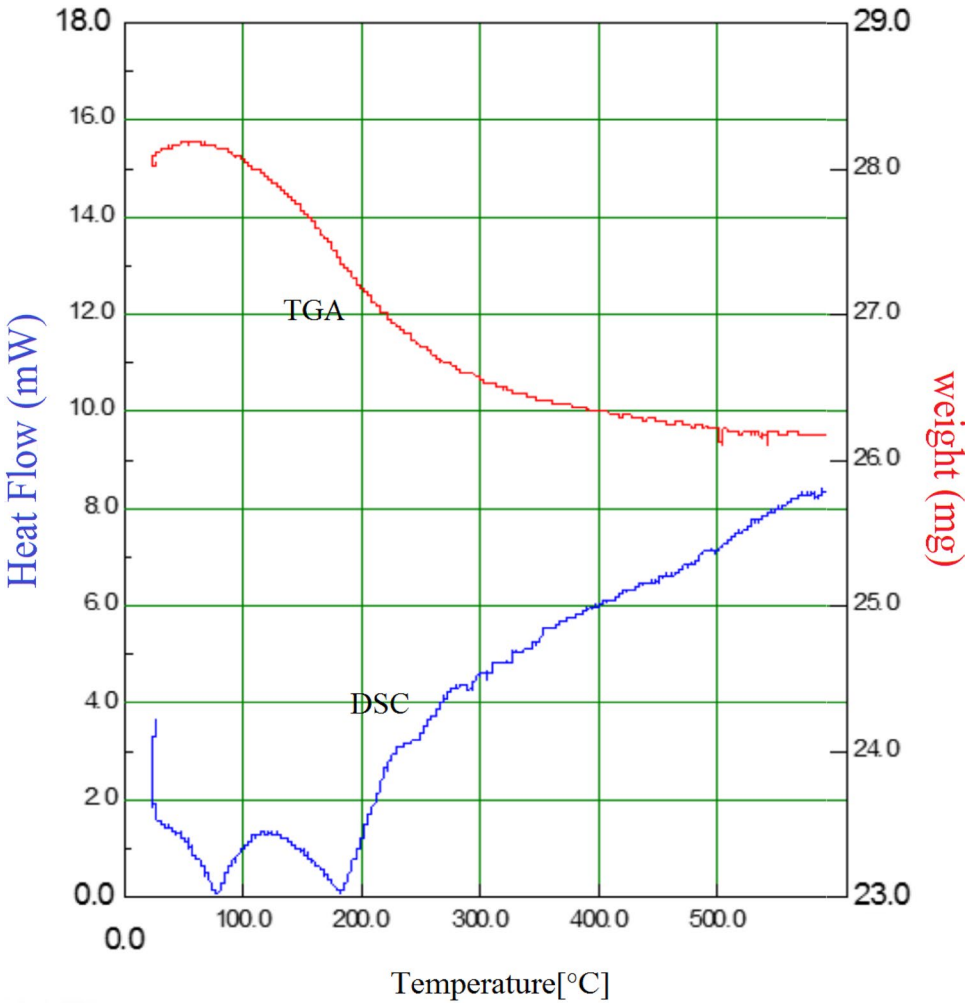

Fig. 8 TGA and DSC curves for (45%Fe–45%Co–10%Ce/60% Zeolite A-3) precursor

Acknowledgements This work is financially and instrumentally supported by the University of Sistan and Baluchestan.

References

1. Sauciuc A, Abosteif Z, Weber G, Potetz A, Rauch R, Hofbauer H, Schaub G, Dumitrescu L (2012) Biomass Convers Biorefin 2:253
2. Ji Y-Y, Xiang H-W, Yang J-L, Xu Y-Y, Li Y-W, Zhong B (2001) Appl Catal 214:77
3. Maitlis PM, de Klerk A (2013) Greener Fischer–Tropsch processes for fuels and feedstocks. Wiley, New York
4. Xu J, Yang Y, Li Y-W (2013) Curr Opin Chem Eng 2:354
5. Akbari M, Mirzaei AA, Atashi H, Arsalanfar M (2018) J Taiwan Inst Chem Eng 91:396
6. Jahangiri H, Bennett J, Mahjoubi P, Wilson K, Gu S (2014) Catal Sci Technol 4:2210
7. Venter J, Kaminsky M, Geoffroy GL, Vannice MA (1987) J Catal 103:450
8. Duvenhage D, Coville N (2005) Appl Catal 289:231
9. Feyzi M, Khodaei MM, Shahmoradi J (2015) Int J Hydrogen Energy 40:14816
10. Liu Y, Teng B-T, Guo X-H, Li Y, Chang J, Tian L, Hao X, Wang Y, Xiang H-W, Xu Y-Y (2007) J Mol Catal A Chem 272:182
11. Van Der Laan GP, Beenackers A (1999) Catal Rev 41:255
12. Hu J, Yu F, Lu Y (2012) Catal 2:303
13. Dry M (1981) Catal Sci Technol 1:159
14. Van de Loosdrecht J, Botes F, Ciobica I, Ferreira A, Gibson P, Moodley D, Saib A, Visagie J, Weststrate C (2013) Fischer–Tropsch synthesis (catalysts and chemistry)
15. Anderson RB, Kölbel H, Rálek M (1984) Academic Press 35:498
16. Özkara-Aydınoğlu Ş, Ataç Ö, Gül ÖF, Kınayyiğit Ş, Şal S, Baranak M, Boz İ (2012) Chem Eng J 181:581
17. Herranz T, Rojas S, Pérez-Alonso FJ, Ojeda M, Terreros P, Fierro JLG (2006) J Catal 243:199
18. Janani H, Rezvani AR, Grivani GH, Mirzaei AA (2015) J Inorg Organomet Polym Mater 5:1169
19. Ma W-P, Ding Y-J, Lin L-W (2004) Ind Eng Chem Res 43:2391
20. Mohamadnasab Omran S, Tavasoli A, Zamani Y (2015) Pet Coal 57:1337
21. Pardo-Tarifa F, Cabrera S, Sanchez-Dominguez M, Boutonnet M (2017) Int J Hydrogen Energy 42:9754
22. Sun B, Lin J, Xu K, Pei Y, Yan S, Qiao M, Zhang X, Zong B (2013) Chem Cat Chem 5:3857
23. Xiong H, Zhang Y, Liew K, Li J (2008) J Mol Catal A Chem 295:68
24. Macheli L, Roy A, Carleschi E, Doyle BP, van Steen E (2018) Catal Today

25. Karandikar PR, Lee YJ, Kwak G, Woo MH, Park SJ, Park H-G, Ha K-S, Jun KW (2014) J Phys Chem C 118:21978
26. Yu L, Liu X, Fang Y, Wang C, Sun Y (2013) Fuel 112:483
27. Sartipi S, Makkee M, Kapteijn F, Gascon J (2014) Catal Sci Technol 4:893
28. Peng X, Cheng K, Kang J, Gu B, Yu X, Zhang Q, Wang Y (2015) Angew Chem Int Ed 54:4553
29. Golestan S, Mirzaei AA, Atashi H (2017) Int J Hydrogen Energy 42:9816
30. Hutchings G, Mirzaei A, Joyner R, Siddiqui M, Taylor S (1998) Appl Catal A 166:143
31. Hutchings GJ, Mirzaei AA, Joyner RW, Siddiqui MRH, Taylor SH (1996) Catal Lett 42:21
32. Mirzaei AA, Shaterian HR, Habibi M, Hutchings GJ, Taylor SH (2003) Appl Catal A 253:499
33. Mirzaei AA, Shaterian HR, Joyner RW, Stockenhuber M, Taylor SH, Hutchings GJ (2003) Catal Commun 4:17
34. Mirzaei AA, Shaterian HR, Kaykhaii M (2005) Appl Surf Sci 239:246
35. Mirzaei AA, Shaterian HR, Taylor SH, Hutchings GJ (2003) Catal Lett 87:103
36. Mirzaei AA, Vahid S, Feyzi M (2008) Adv Phys Chem 1:1687
37. Taylor SH, Hutchings GJ, Mirzaei AA (1999) Chem Commun 1:1373
38. Taylor SH, Hutchings GJ, Mirzaei AA (2003) Catal Today 84:113
39. Whittle DM, Mirzaei AA, Hargreaves JS, Joyner RW, Kiely CJ, Taylor SH, Hutchings GJ (2002) Phys Chem Chem Phys 4:5915
40. Moradi G, Basir M, Taeb A, Kiennemann A (2003) Catal Commun 4:27
41. Parlett CM, Bruce DW, Hondow NS, Lee AF, Wilson K (2011) ACS Catal 1:636
42. Feyzi M, Mirzaei AA, Bozorgzadeh HR (2010) J Nat Gas Chem 19:341
43. Barrault J, Forquy C, Perrichon V (1983) Appl Catal 5:119
44. Krishna KR, Bell AT (1993) J Catal 139:104
45. Pendyala VRR, Shafer WD, Jacobs G, Davis BH (2014) Catal Lett 144:1088
46. Atashi H, Siami F, Mirzaei A, Sarkari M (2010) J Ind Eng Chem 16:952
47. Gaube J, Herzog K, König L, Schliebs B (1986) Chem Ing Tech 58:682
48. Choudhury HA, Moholkar VS (2013) Int J Sci Eng Technol 2:31
49. Jalama K (2015) Proceedings of the World Congress on engineering and computer science
50. Yang JH, Kim H-J, Chun DH, Lee H-T, Hong J-C, Jung H, Yang J-I (2010) Fuel Process Technol 91:285
51. Bukur DB, Lang X, Akgerman A, Feng Z (1997) Ind Eng Chem Res 36:2580
52. Madon RJ, Iglesia E (1993) J Catal 139:576
53. Tristantini D, Lögdberg S, Gevert B, Borg Ø, Holmen A (2007) Fuel Process Technol 88:643
54. Abbaslou RMM, Mohammadzadeh JSS, Dalai AK (2009) Fuel Process Technol 90:849
55. Kim S-M, Bae JW, Lee Y-J, Jun K-W (2008) Catal Commun 9:2269
56. Park C, Baker R (2000) J Catal 190:104
57. Caeiro G, Carvalho R, Wang X. Lemos M, Lemos F, Guisnet M, Ribeiro F (2006) J Mol Catal A Chem 255:131
58. Bolton AP (1976) Hydrocracking, isomerization and other industrial processes. American Chemical Society, Washington DC
59. Chen N, Garwood W (1986) Catal Rev Sci Eng 28:185
60. Corma A (1995) Chem Rev 95:559
61. Arsalanfar M, Mirzaei AA, Bozorgzadeh HR, Atashi H, Shahriari S (2012) J Nat Gas Sci Eng 9:119